IOPscience iopscience.iop.org

Home Search Collections Journals About Contact us My IOPscience

Characteristics of MOCVD- and MBE-grown InGa(N)As VCSELs

This content has been downloaded from IOPscience. Please scroll down to see the full text.

2005 Semicond. Sci. Technol. 20 834

(http://iopscience.iop.org/0268-1242/20/8/035)

View the table of contents for this issue, or go to the journal homepage for more

Download details:

IP Address: 140.113.38.11
This content was downloaded on 26/04/2014 at 11:51

Please note that terms and conditions apply.

Semicond. Sci. Technol. **20** (2005) 834–839 doi:10.1088/0268-1242/20/8/035

Characteristics of MOCVD- and MBE-grown InGa(N)As VCSELs

H-P D Yang[1], C Lu[1], R Hsiao[2], C Chiou[1], C Lee[1], C Huang[1], H Yu[3], C Wang[1], K Lin[1], N A Maleev[4], A R Kovsh[4], C Sung[1], C Lai[1], J Wang[1], J Chen[2], T Lee[1] and J Y Chi[1]

[1] Nanophotonics Center, Opto-Electronics & Systems Laboratories, Industrial Technology Research Institute, Chutung 310, Hsinchu, Taiwan
[2] Department of Electrophysics, National Chiao Tung University, Hsinchu 300, Taiwan
[3] Institute of Microelectronics, National Cheng Kung University, Tainan 701, Taiwan
[4] A F Ioffe Physico-Technical Institute, St. Petersburg 194021, Russia

E-mail: hpyang@itri.org.tw

Received 24 September 2004, in final form 1 June 2005
Published 11 July 2005
Online at stacks.iop.org/SST/20/834

Abstract
We report our results on InGaNAs/GaAs vertical-cavity surface-emitting lasers (VCSELs) in the 1.3 μm range. The epitaxial structures were grown on (1 0 0) GaAs substrates by metalorganic chemical vapour deposition (MOCVD) or molecular beam epitaxy (MBE). The nitrogen composition of the InGa(N)As/GaAs quantum-well (QW) active region is 0–0.02. The long-wavelength (up to 1.3 μm) room-temperature continuous-wave (RT CW) lasing operation was achieved for MBE- and MOCVD-grown VCSELs. For MOCVD-grown devices with n- and p-doped distributed Bragg reflectors (DBRs), a maximum optical output power of 0.74 mW was measured for $In_{0.36}Ga_{0.64}N_{0.006}As_{0.994}$/GaAs VCSELs. A very low J_{th} of 2.55 kA cm^{-2} was obtained for the InGaNAs/GaAs VCSELs. The MBE-grown devices were made with an intracavity structure. Top-emitting multi-mode 1.3 μm $In_{0.35}Ga_{0.65}N_{0.02}As_{0.98}$/GaAs VCSELs with 1 mW output power have been achieved under RT CW operation. A J_{th} of 1.52 kA cm^{-2} has been obtained for the MBE-grown $In_{0.35}Ga_{0.65}N_{0.02}As_{0.98}$/GaAs VCSELs, which is the lowest threshold current density reported. The emission characteristics of the InGaNAs/GaAs VCSELs were measured and analysed.

1. Introduction

Vertical-cavity surface-emitting lasers (VCSELs) are attractive low-cost light emitters for fibre-optic communications. The advantages of VCSELs include lower threshold current, smaller beam divergence angle, higher optical fibre coupling efficiency and on-wafer testability, as compared to edge-emitting lasers. AlGaAs/GaAs VCSELs and VCSEL-based transceivers operating at 850 nm have been implemented in gigabit ethernet (GbE) and fibre channel links. These VCSELs have a shorter transmission distance of about 500 m over multimode fibres. For longer transmission distances (>1 km), 1.3 and 1.55 μm Fabry–Perot (FP) and distributed feedback (DFB) lasers are commonly used because of lower dispersion in the optical fibre. VCSELs operating at the 1.3–1.55 μm range have the potential for both short- and long-reach fibre-optic communications. Other applications may include sensing and optical interconnects. A number of material systems have been studied, including InAs quantum dots [1], wafer-fused InGaAsP–InP [2, 3], InAlGaAs/InP [4] and GaAsSb/GaAs VCSELs [5]. InGaNAs material systems grown on GaAs substrates have drawn a lot of attention because they can achieve light emission in the 1.3 μm range [6]. In addition, epitaxially grown AlGaAs/GaAs distributed Bragg reflectors can be used as reflecting mirrors for the GaAs-based VCSELs. Compared to that of the 980 nm $In_{0.2}Ga_{0.8}As$/GaAs VCSELs, the InGaNAs/GaAs VCSELs can lase with longer emission wavelengths by incorporating higher indium composition and nitrogen in the QW active region during growth. High-performance InGaAs

0268-1242/05/080834+06$30.00 © 2005 IOP Publishing Ltd Printed in the UK

and InGaNAs edge-emitting Fabry–Perot lasers have also been demonstrated [7–10]. The InGaNAs lasers showed better temperature stability than that of the InP-based lasers [11]. Moreover, a number of InGaNAs VCSEL results have been reported very recently [12–14]. In this work, we have made InGaNAs/GaAs and InGaAs/GaAs VCSELs for fibre-optic applications in the 1.3 μm range. Two approaches have been investigated. One approach is the devices made with the conventional top-emitting structure, while the other approach is the devices made with the intracavity-contacted structure. The epitaxial layers were monolithically grown on (1 0 0) GaAs substrates either by metalorganic chemical vapour deposition (MOCVD) or by molecular beam epitaxy (MBE). The devices have demonstrated a maximum optical output power of over 1 mW, with a low threshold current density of 1.53 kA cm^{-2} at 1.3 μm. The emission characteristics of the InGaAs and InGaNAs VCSELs were measured and analysed.

2. Epitaxial growth and device fabrication

2.1. MOCVD-grown InGaAs and InGaNAs VCSELs

The epitaxial layers of the InGaNAs/GaAs and InGaAs/GaAs VCSELs were grown on two-inch (1 0 0) n$^+$-GaAs substrates by an AIXTRON 200 MOCVD system. The gas sources include trimethylgallium (TMGa), trimethylaluminium (TMAl), trimethylindium (TMIn), dimethylhydrazine (DMHy) and tertiarybutylarsine (TBA). The epitaxial structure is the following (from bottom to top): a n$^+$-GaAs buffer, a 40.5-pair n$^+$-$Al_{0.9}Ga_{0.1}As$/n$^+$-GaAs (Si-doped) distributed Bragg reflector (DBR), an undoped $InGaN_yAs_{1-y}$/GaAs active region, a p-$Al_{0.98}Ga_{0.02}As$ oxidation layer, a 25-pair p$^+$-$Al_{0.9}Ga_{0.1}As$/p$^+$-GaAs DBR (carbon doped) and a p$^+$-GaAs (carbon doped) contact layer. The graded-index separate confinement heterostructure (GRINSCH) active region mainly consists of two undoped $InGaN_yAs_{1-y}$/GaAs ($0 \leqslant y \leqslant 0.01$) quantum wells embedded between two linear-graded undoped $Al_xGa_{1-x}As$ (x = 0–0.6 and x = 0.6–0) confinement layers. The thickness of the $InGaN_yAs_{1-y}$ well layer is 6–7 nm. The total thickness of the cavity active region is 1λ. The p-type and n-type distributed Bragg reflectors (DBRs) of the VCSEL consist of alternating $Al_{0.9}Ga_{0.1}As$/GaAs quarter-wave ($\lambda/4$) stacks. Carbon was used as the p-type dopant in the DBR to obtain higher carrier concentration (2–3 $\times$ 10^{18} cm^{-3}), in order to reduce the series resistance of the p-DBR layers. The interfaces of both the p-type and n-type $Al_{0.9}Ga_{0.1}As$/GaAs DBR layers are linearly graded, also to reduce the series resistance. The reflectance spectra of the grown VCSEL wafers were also measured. The cavity resonance was in the 1100–1300 nm range, depending on the composition of indium and nitrogen in the active region of each grown wafer. The composition of the grown layer was estimated from the rocking curve of the x-ray diffraction (XRD) spectrum. Photoluminescence (PL) measurements were done by using a Bio-Rad mapping system. The PL emission peaks of the grown InGaNAs/GaAs VCSEL epi-wafers were from 1150 to 1270 nm. As shown in figure 1, the typical PL peak emission wavelengths (λ_p) of the two grown $In_{0.36}Ga_{0.64}As$/GaAs and $In_{0.36}Ga_{0.64}N_{0.006}As_{0.994}$/GaAs QW VCSEL epi-wafers are 1150 and 1260 nm, respectively. The peak emission wavelength difference is 112 nm. Compared to the $In_{0.36}Ga_{0.64}As$ VCSELs, the $In_{0.36}Ga_{0.64}N_{0.006}As_{0.994}$ VCSEL epi-layers emit with longer PL wavelength, but with lower PL intensity. The full-width half maximum (FWHM) of the PL emission peak is larger. PL measurements of all the InGaNAs VCSEL wafers also showed that with higher nitrogen content in the InGaNAs QWs, the PL peak wavelength was longer, and the PL intensity was lower. This trend may be due to more alloy scattering in the quaternary InGaNAs layers than in the ternary InGaAs layers in the active region.

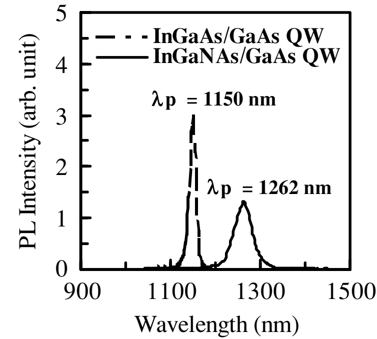

Figure 1. PL spectra of $In_{0.36}Ga_{0.64}As$ and $In_{0.36}Ga_{0.64}N_{0.006}As_{0.994}$ VCSEL epi-layers.

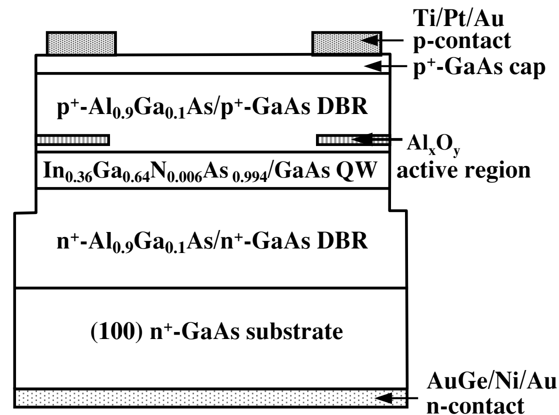

Figure 2. Schematic diagram of $In_{0.36}Ga_{0.64}N_{0.006}As_{0.994}$/GaAs VCSEL made with conventional device structure.

The top-emitting VCSEL fabrication processes are described as follows. Firstly, a mesa was formed by using a reactive ion etch (RIE). Then, selective oxidation was performed at 425 °C in an oxidation furnace under nitrogen flow with steam. The oxide aperture size was about 8–25 μm in diameter. The p-Ohmic contacts, which defined the light-emitting windows, were formed by evaporating Ti/Pt/Au. After that, the AuGe/Ni/Au n-Ohmic was formed at the backside of the substrate. The pad metal was then evaporated to facilitate probing and bonding. The schematic diagram of the $In_{0.36}Ga_{0.64}N_{0.006}As_{0.994}$/GaAs VCSEL is shown in figure 2

2.2. MBE-grown intracavity-contacted InGaNAs VCSELs

The intracavity VCSEL structures were grown by a Riber Epineat MBE system with a Uni-Bulb RF plasma source

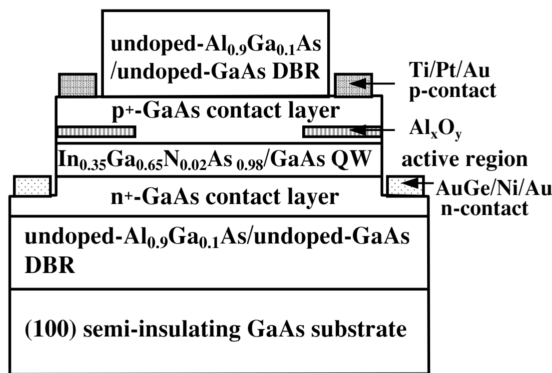

Figure 3. Schematic diagram of intracavity-contacted $In_{0.35}Ga_{0.65}N_{0.02}As_{0.98}$ VCSEL.

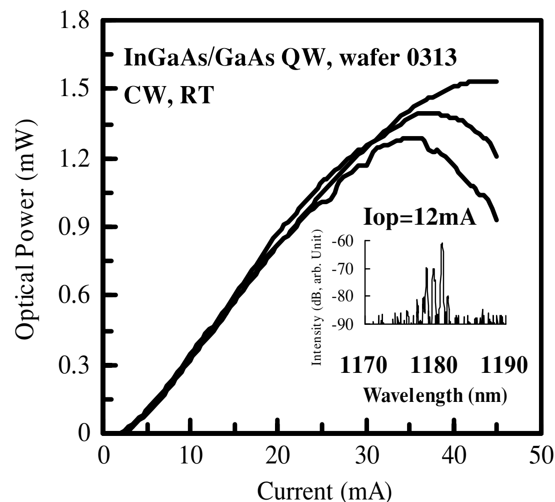

Figure 4. Optical output power versus current characteristics and optical spectrum (inset) of a 22 μm aperture $In_{0.36}Ga_{0.64}As$/GaAs VCSEL (wafer 0313).

to generate reactive nitrogen from ultra-pure N_2 gas. The intracavity p^+–i–n^+ structure design was chosen to avoid free carrier absorption in p-doped DBRs. The DBR layers were undoped-AlGaAs/undoped-GaAs pairs. The active region consists of two 6 nm/12 nm $In_{0.35}Ga_{0.65}N_{0.02}As_{0.98}$/GaAs QWs. The growth temperature of the active region was 420 °C to avoid phase separation effects. After growing a 55 nm $Al_{0.98}Ga_{0.02}As$ current-confinement aperture layer, the wafer was *in situ* annealed at 750 °C for 10 min to remove point defects formed in the active region during low temperature growth. The total cavity thickness was 5λ (1888 nm), including an undoped 1-λ (377.6 nm) GaAs layer with InGaNAs/GaAs double QWs. p^+-GaAs and n^+-GaAs contact layers were grown on top and bottom of the active region, respectively. Beryllium and silicon were used as p- and n-type dopants for the contact layers. Three heavily Be-doped p^+-GaAs layers were located at the minima of the optical field in the p^+-GaAs contact layers to reduce the series resistance and to improve the current spreading uniformity. The top and bottom mirrors consist of 25 and 33 pairs of undoped-$Al_{0.9}Ga_{0.1}As$/undoped-GaAs quarter-wave stacks, respectively. The epitaxial layers were grown on semi-insulating (1 0 0) GaAs substrates.

The intracavity-contacted VCSELs were made with double-mesa processes. Firstly, the top and bottom mesas were formed by using RIE and selective wet chemical etch, so that the etched surfaces for p-type and n-type Ohmic contacts stopped at the p^+- and n^+-GaAs contact layers, respectively. Next, the device aperture was defined by wet oxidation. Then, p-type and n-type Ohmic contacts were formed on the p^+- and n^+-GaAs contact layers by electron beam evaporation and annealing. After that, the devices were passivated by SiO_2. The pad metal was evaporated to facilitate probing and bonding. The device structure is shown schematically in figure 3.

3. Results and discussions

3.1. MOCVD-grown InGaAs and InGaNAs VCSELs

The lasing wavelength and optical power distribution were measured by a wafer-scale probing. The spectra of the InGaAs/GaAs and InGaNAs/GaAs VCSELs were measured by an Advantest Q8381A optical spectrum analyser. These devices showed multiple transverse mode characteristics. The InGaAs/GaAs VCSELs showed lasing wavelengths ranging from 1160 to 1250 nm, while the InGaNAs/GaAs VCSELs showed lasing wavelengths ranging from 1210 to 1310 nm. The InGaNAs VCSELs emit at longer wavelengths than the InGaAs VCSELs for devices with the same indium and gallium contents in the QWs.

The room-temperature (RT) optical power versus current (*L–I*) characteristics and optical spectrum (inset) of the $In_{0.36}Ga_{0.64}As$/GaAs VCSEL (wafer 0313) are shown in figure 4. The oxide apertures of these devices are approximately 22 μm. The threshold currents (I_{th}) are approximately 1.5 mA, which are converted to very low threshold current densities (J_{th}) of 395 A cm^{-2}. The peak emission wavelength (inset) is 1180 nm. The slope efficiency of the *L–I* curves is approximately 0.05 W A^{-1}. A maximum continuous-wave (CW) optical power of 1.53 mW was measured at room temperature. The output power rollover occurs as the current increases beyond 37–45 mA. The overall emission peak wavelengths of devices on the wafer (wafer 0313) are 1160–1180 nm at 12 mA. The higher indium content of the InGaAs QWs can lead to smaller bandgap, and therefore longer lasing wavelengths. By increasing the indium content in the InGaAs QWs to 0.39 (wafer 1111), a peak lasing wavelength of 1250 nm can be achieved (shown in figure 5). The PL emission wavelength for wafer 1111 is 1180 nm. The cavity resonance obtained from the reflectance measurement is 1250 nm. Despite that the large detuning between PL/gain peak and cavity resonance is about 70 nm; the InGaAs VCSELs were able to lase up to 1250 nm. For InGaAs VCSELs, the optical power decreases with increasing indium content in the QWs. This trend may be due to very high strain in the QWs that degrade the output power of the devices.

The room-temperature *L–I* characteristics of the $In_{0.36}Ga_{0.64}N_{0.006}As_{0.994}$/GaAs VCSELs (wafer 0319) are shown in figure 6. The oxide apertures of the devices are

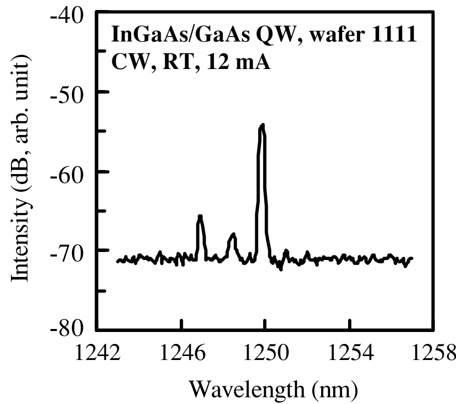

Figure 5. Optical spectrum of an $In_{0.39}Ga_{0.41}As/GaAs$ VCSEL (wafer 1111) at 12 mA.

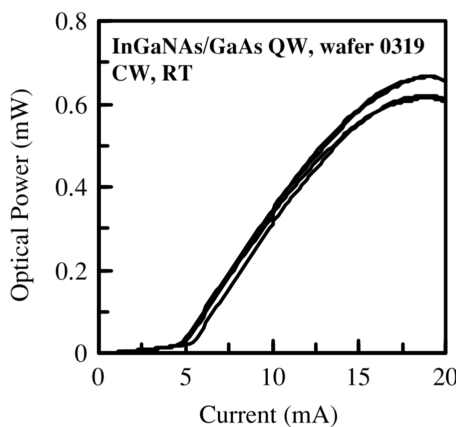

Figure 6. Optical power versus current characteristics of a 10 μm aperture $In_{0.36}Ga_{0.64}N_{0.006}As_{0.994}/GaAs$ VCSEL (wafer 0319).

10 μm in diameter. The threshold currents of these devices are approximately 4.5 mA, which are converted to threshold current densities, J_{th}, of approximately 5.7 kA cm^2. This J_{th} value, compared to those of the InGaAs VCSELs, is higher corresponding to a lower PL intensity of the grown InGaNAs VCSEL wafer. The peak emission wavelengths of these devices on this wafer (wafer 0319) were 1190–1230 nm. As shown in figure 6, a maximum CW optical output power of 0.68 mW was measured at 19 mA. The slope efficiency is approximately 0.065 W A^{-1}. The differential series resistances of the devices are low, approximately 58 Ω at 10 mA, with a threshold voltage of 1.0 V. A maximum optical output power of 0.74 mW was measured by a wafer-scale probing. The room-temperature *L–I* characteristics and optical spectrum (inset) of the $In_{0.36}Ga_{0.64}N_yAs_{1-y}/GaAs$ VCSELs (on wafer 0328) are shown in figure 7. The nitrogen composition (y) is estimated to be approximately 0.0065. The threshold currents of these devices are 3.1–3.7 mA, which are converted to threshold current densities of 4.0–4.7 kA cm^{-2}. The optical power rollovers occur approximately at 13–15 mA, with a maximum power of 0.44 mW. The peak emission wavelength is 1240 nm at 10 mA. The photograph of a lasing InGaNAs VCSEL (on wafer 0328) probed at 4 mA is shown in figure 8. Figure 9 shows the temperature-dependent *L–I* characteristics of an InGaNAs/GaAs VCSEL

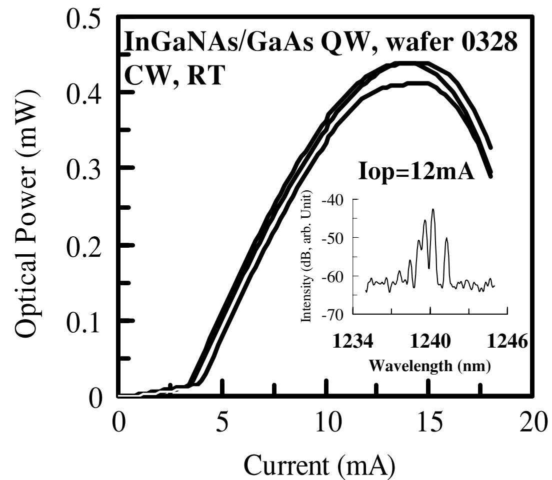

Figure 7. Optical power versus current characteristics and optical spectrum (inset) of the $In_{0.36}Ga_{0.64}N_yAs_{1-y}/GaAs$ VCSEL (wafer 0328), $y = 0.0065$.

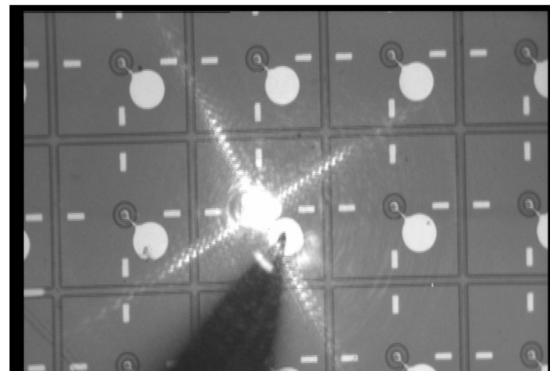

Figure 8. Photograph of the InGaNAs VCSELs (wafer 0328) with one of the devices probed at 4 mA.

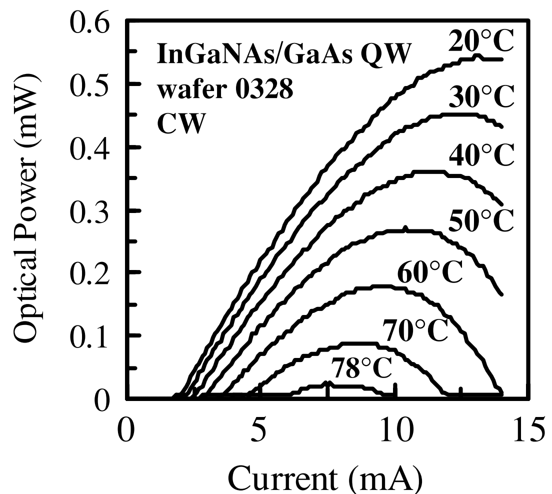

Figure 9. Temperature-dependent optical power versus current characteristics of the InGaNAs/GaAs VCSEL (wafer 0328).

(on wafer 0328). The device demonstrates CW operation up to 78 °C. The threshold current increases with increasing temperature, from 2 mA at 20 °C to 6 mA at 78 °C. The

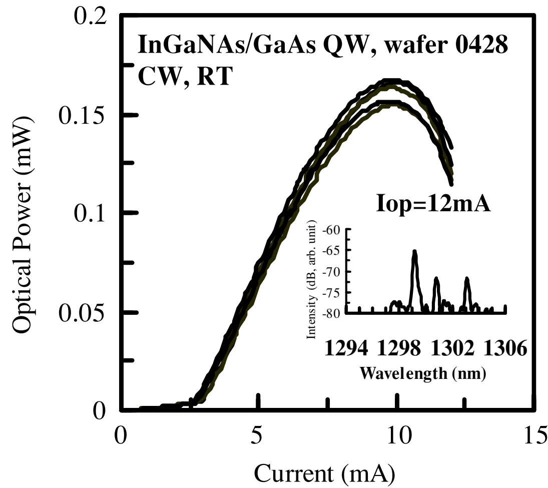

Figure 10. Optical power versus current characteristics and optical spectrum (inset) of the $In_{0.36}Ga_{0.64}N_{0.007}As_{0.993}$/GaAs VCSEL (wafer 0428).

threshold current density, J_{th}, is approximately 2.55 kA cm^{-2} at 20, with a maximum optical power of 0.55 mW. This J_{th} is one of the lowest threshold current densities measured [12–14, 16]. A maximum lasing wavelength of 1310 nm was measured for the $In_{0.36}Ga_{0.64}N_{0.007}As_{0.993}$/GaAs VCSELs (wafer 0428) by using a wafer-scale probing of the devices. The *L–I* characteristics and optical spectrum (inset) of the $In_{0.36}Ga_{0.64}N_{0.007}As_{0.993}$/GaAs VCSEL are shown in figure 10. The peak emission wavelengths are 1299–1303 nm at 12 mA. The threshold currents are approximately 2.7 mA, which are converted to threshold current densities of approximately 3.44 kA cm^{-2} for 10 μm aperture devices. In summary, CW lasing operations have been demonstrated for the InGaAs/GaAs and InGaNAs/GaAs VCSELs at room temperature up to 1303 nm. The devices show multiple transverse mode characteristics. For most devices, higher optical output power can be achieved with shorter lasing wavelengths. Higher indium or nitrogen contents in the InGaAs/GaAs and InGaNAs/GaAs QWs of the VCSELs result in longer emission wavelengths. More indium content in the QWs also leads to higher strain, which may degrade the output power of the devices.

3.2. MBE-grown intracavity-contacted InGaNAs VCSELs

Figure 11 shows optical power–current–voltage curves of VCSEL with an 18 μm aperture. The near-field pattern and optical spectrum (insets) of the device driven above I_{th} are also shown. The peak lasing wavelength is 1304 nm. The threshold current (I_{th}) is 4 mA with a forward voltage of 2.5 V. The threshold current density is 1.58 kA cm^{-2}, which is the lowest value reported for InGaAsN/GaAs QW VCSELs. Figures 12(*a*) and (*b*) show the temperature-dependent optical power–current characteristics of the InGaNAs VCSEL with pulsed and CW operations, respectively. They show pulsed operation up to 95 °C, while CW operation up to 50 °C. The output power is more than 10 mW, with a slope efficiency of about 0.20 W A^{-1} under pulsed operation. Multi-mode CW output power exceeding 1 mW with a slope efficiency of 0.15 W A^{-1} was

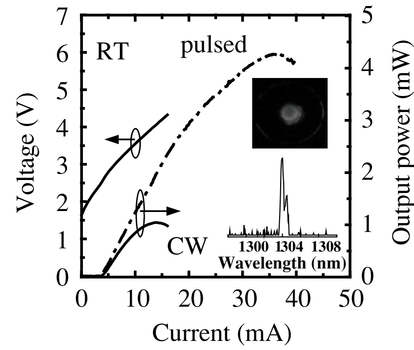

Figure 11. Room temperature optical power–current–voltage curves of the intracavity-contacted $In_{0.35}Ga_{0.65}N_{0.02}As_{0.98}$/GaAs VCSEL with an 18 μm aperture. The near-field pattern and optical spectrum of the device driven above I_{th} are also included (inset).

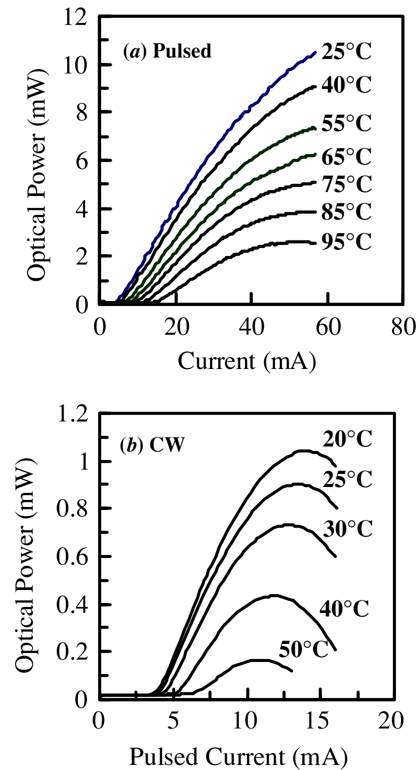

Figure 12. Temperature-dependent (*a*) pulsed and (*b*) CW optical power versus current characteristics of the intracavity-contacted $In_{0.35}Ga_{0.65}N_{0.02}As_{0.98}$/GaAs VCSEL.

achieved. In spite of high quality of the active region, the device performance is limited by the thermal heating effect. We believe that significant improvement in the VCSEL performance can be done by further optimization of the VCSEL structure design and the processing procedure.

The temperature dependence of the threshold current is shown in figure 13. CW operation is maintained up to 50 °C. The minimum threshold current obtained by extrapolation is well below room temperature. This indicates the non-optimal detuning of gain peak and cavity resonance. Thus, minimizing the detuning of the gain peak and cavity resonance can result in longer emission wavelength, higher output

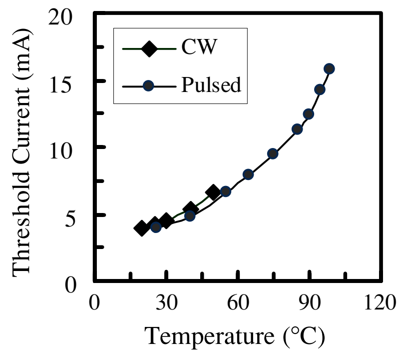

Figure 13. Temperature-dependent pulsed and CW threshold current of the intracavity-contacted $In_{0.35}Ga_{0.65}N_{0.02}As_{0.98}/GaAs$ VCSEL.

power and better high-temperature performance in future devices.

3.3. Comparison of the MOCVD- and MBE-grown InGaNAs VCSELs

For the MOCVD-grown InGaAs VCSELs, the output power decreases with increasing indium content in the QWs. This is mainly because of the increasing strain in the QWs that degrades the epitaxial layer quality and the output power of the devices. The lasing wavelength was up to 1250 nm for the $In_xGa_{1-x}As$ VCSELs with $x = 0.39$. For both our $In_xGa_{1-x}As$ and $In_xGa_{1-x}NAs$ VCSELs, the lattice mismatches are higher, 2.51% for $x = 0.35$ and 2.87% for $x = 0.40$. The critical thickness of the $In_xGa_{1-x}As$ layer on GaAs is 67 Å for $x = 0.35$ and is 56 Å for $x = 0.40$, by using a theoretical calculation [15]. To achieve longer laser emission wavelength in the 1.3 μm range, thicker InGaAs or InGaNAs quantum well layers beyond the theoretical critical thickness were grown. The growth of a high quality InGaNAs layer is an important issue; the overall PL intensity of the MOCVD-grown InGaNAs VCSEL wafer is lower than that of the InGaAs wafers (shown in figure 1). To avoid more problems from the strain, the $In_xGa_{1-x}NAs$ layers were grown with $x = 0.36$, while the nitrogen content varied from 0.006 to 0.007. The MOCVD-grown InGaNAs VCSELs were able to lase up to 1310 nm, but with lower output power. This indicates the point defects in the QW layers due to the incorporation of nitrogen, which dominate the device properties. For the MBE-grown InGaNAs VCSEL wafer, an additional high temperature annealing under arsenic overpressure was made to remove the point defects in the QW layers during low temperature growth. For longer lasing wavelengths near 1.3 μm, the output powers of the MOCVD-grown VCSELs are lower than those of the MBE-grown devices, which may also be due to free carrier absorption in the heavily p-type doped DBR layers. Moreover, strain-compensated InGaNAs/GaAsP QWs could be another approach to solve the strain problem of the device [9].

4. Conclusion

In conclusion, continuous-wave lasing operations of InGaNAs/GaAs and InGaAs/GaAs VCSELs in the 1.3 μm range have been demonstrated at room temperature. The epitaxial layers were grown by MOCVD and MBE. For MOCVD-grown devices with doped DBRs, maximum optical powers of 1.5 and 0.74 mW have been measured for the InGaAs/GaAs and InGaNAs/GaAs VCSELs, respectively. A very low J_{th} of 2.55 kA cm^{-2} was obtained for the InGaNAs/GaAs VCSELs. MBE-grown 1.3 μm intracavity-contacted InGaNAs/GaAs VCSELs with 1 mW output power were demonstrated. A J_{th} of 1.52 kA cm^{-2} has been obtained for the MBE-grown $In_{0.35}Ga_{0.65}N_{0.02}As_{0.98}/GaAs$ VCSELs, which is the lowest threshold current density reported. These InGaAs and InGaNAs VCSELs are suitable for fibre-optic applications. Future improvement of the devices can be made by minimizing the detuning of cavity resonance and the gain peak.

Acknowledgments

The authors would like to thank Dr D Livchitz for useful discussions. This work was supported by Epitaxial Light Source, Nanophotonic Technology Projects, and ITRI-Ioffe Joint Scientific Program, MOEA, Taiwan.

References

[1] Lott J A, Ledentsov N N, Ustinov V M, Maleev N A, Zhukov A E, Kovsh A R, Maximov M V, Volovik B V, Alferov Z H I and Bimberg D 2000 *Electron. Lett.* **36** 1384
[2] Okuno Y L, Geske J, Gan K, Chiu Y, Denbaars S P and Bowers J E 2000 *Appl. Phys. Lett.* **82** 2377
[3] Karim A, Abraham P, Lofgreen D, Chiu Y J, Piprek J and Bowers J E 2001 *Appl. Phys. Lett.* **78** 2632
[4] Shin J, Kim J, Song H, Han I, Ju Y, Han W and Kwon O 2003 *Electron. Lett.* **39** 664
[5] Quochi F, Kilper D, Cunningham J, Dinu M and Shah J 2001 *IEEE Photon. Technol. Lett.* **13** 921
[6] Kondow M, Kitatani T, Nakatsuka S, Larson M C, Nakahara K, Yazawa Y, Okai M and Uomi K 1997 *IEEE J. Sel. Top. Quantum Electron.* **3** 719
[7] Sato S 2000 *Japan. J. Appl. Phys.* **39** 3403
[8] Nakahara K, Kondow M, Kitanani T, Larson M C and Uomi K 1998 *IEEE Photon. Technol. Lett.* **10** 487
[9] Tansu N and Mawst L J 2002 *IEEE Photon. Technol. Lett.* **14** 444
[10] Mogg S, Chitica N, Schatz R and Hammar M 2002 *Appl. Phys. Lett.* **81** 2334
[11] Illek S, Ultsch A, Borchert B, Egorov A Y and Riechert H 2000 *Electron. Lett.* **36** 725
[12] Larson M C, Coldren C W, Spruytte S G, Petersen H E and Harris J S 2000 *IEEE Photon. Technol. Lett.* **12** 1598
[13] Takeuchi T, Chang Y-L, Leary M, Tandon A, Luan H-C, Bour D, Corzine S, Twist S R and Tan M 2002 *Electron. Lett.* **38** 1438
[14] Ramakrishnan A, Steinle G, Supper D, Degen C and Ebbinghaus G 2002 *Electron. Lett.* **38** 322
[15] Jaffe M and Singh J 1989 *J. Appl. Phys.* **65** 329
[16] Vukusic J *et al* 2003 *Electron. Lett.* **39** 662